

Tropical Pacific impacts of convective momentum transport in the SNU coupled GCM

Daehyun Kim · Jong-Seong Kug · In-Sik Kang ·
Fei-Fei Jin · Andrew T. Wittenberg

Received: 4 August 2007 / Accepted: 26 November 2007
© Springer-Verlag 2007

Abstract Impacts of convective momentum transport (CMT) on tropical Pacific climate are examined, using an atmospheric (AGCM) and coupled GCM (CGCM) from Seoul National University. The CMT scheme affects the surface mainly via a convection-compensating atmospheric subsidence which conveys momentum downward through most of the troposphere. AGCM simulations—with SSTs prescribed from climatological and El Niño Southern Oscillation (ENSO) conditions—show substantial changes in circulation when CMT is added, such as an eastward shift of the climatological trade winds and west Pacific convection. The CMT also alters the ENSO wind anomalies by shifting them eastward and widening them meridionally, despite only subtle changes in the precipitation anomaly patterns. During ENSO, CMT affects the low-level winds mainly via the anomalous convection acting on the climatological westerly wind shear over the central Pacific—so that an eastward shift of convection transfers more westerly momentum toward the surface than would occur without CMT. By altering the low-level

circulation, the CMT further alters the precipitation, which in turn feeds back on the CMT. In the CGCM, CMT affects the simulated climatology by shifting the mean convection and trade winds eastward and warming the equatorial SST; the ENSO period and amplitude also increase. In contrast to the AGCM simulations, CMT substantially alters the El Niño precipitation anomaly patterns in the CGCM. Also discussed are possible impacts of the CMT-induced changes in climatology on the simulated ENSO.

1 Introduction

Atmospheric convection is the primary heat source driving the atmospheric circulation, and modulates that circulation by transporting momentum vertically (Wu and Yanai 1994; Tung and Yanai 2002a, b). Called “cumulus friction” in earlier studies (Helfand 1979; Thompson and Hartmann 1979), this convective momentum transport (hereafter, CMT) plays an important role in the atmospheric momentum budget (Stevens 1979; Carr and Bretherton 2001; Tung and Yanai 2002a, b; Lin et al. 2005; Dima et al. 2005). Recently, Lin et al. (2007) calculated the momentum budget of the climatological Walker circulation using two reanalysis datasets, and concluded that CMT is important in both deep (80–160°E) and shallow convection (180–120°W) regions. Nevertheless, many state-of-the-art climate models omit this process.

Numerical representations of CMT have been developed for climate models (Zhang and Cho 1991; Wu and Yanai 1994; Kershaw and Gregory 1997) and used to examine the impact of CMT on climate simulations. Tiedtke (1989) showed that including a simple parameterization of CMT improved the simulation of upper level rotational flow. In

D. Kim · I.-S. Kang
School of Earth and Environmental Sciences,
Seoul National University, Seoul, South Korea

J.-S. Kug · I.-S. Kang (✉)
Climate Environmental System Research Center,
Seoul National University, Seoul, South Korea
e-mail: kang@climate.snu.ac.kr

F.-F. Jin
Department of Meteorology, SOEST,
University of Hawaii, Honolulu, USA

A. T. Wittenberg
Geophysical Fluid Dynamics Laboratory,
NOAA, Princeton, USA

the Tiedtke study, which neglected effects of convective-scale pressure gradient forces, the CMT produced little change in the simulated Hadley circulation. More recent studies, which have included this pressure gradient effect, have found varying impacts on the Hadley circulation—with some showing a strengthening (Zhang and McFarlane 1995; Gregory et al. 1997) and others a weakening (Wu et al. 2003, 2007).

In addition, Wu et al. (2003) have shown that CMT plays a crucial role in simulating the seasonal migration of the ITCZ across the equator. They found that a CMT-induced secondary meridional circulation weakens the Hadley circulation, especially in boreal winter. By suppressing precipitation near the equator, and enhancing off-equatorial rainfall in boreal winter when the ITCZ is far from the equator, CMT improves the model's seasonal migration of the ITCZ.

While many studies have focused on the impact of CMT in simulating the climatology and its seasonal cycle, it is not yet clear exactly how CMT affects ENSO. Some modeling centers have found CMT to strongly affect their coupled GCM ENSO simulations—generating stronger amplitudes and shifting the ENSO spectrum towards longer periods (Wittenberg et al. 2003; Neale 2007). Wittenberg et al. (2003) postulated that by altering the central longitude and meridional width of the anomalous wind stress response to ENSO SST anomalies, CMT affects the time scale for oceanic adjustment and therefore ENSO. Indeed the link between the structure of the wind stress coupling and the behavior of ENSO has been demonstrated in both intermediate models (Cane et al. 1990; Kirtman 1997; An and Wang 2000) and coupled GCMs (Zelle et al. 2005; Capotondi et al. 2006). In this study, we implement a CMT parameterization in both atmosphere-only and atmosphere–ocean coupled GCMs at SNU, and show how the CMT alters the wind stress coupling and the simulated ENSO.

The main questions addressed by this paper are: (1) Does including CMT affect the simulated atmospheric response to SST ENSO forcing? and (2) If so, how?

In the following section, descriptions for implemented CMT scheme, experimental design and observational data are given. The effects of CMT on the response of

atmosphere to the El Niño SST anomaly are investigated using the AGCM perpetual simulations in Sect. 3. In Sect. 4, the results from multi-decadal coupled model simulations are shown. Summary and discussion are presented in Sect. 5.

2 Method, experimental design and data

2.1 Convective momentum transport parameterization

The CMT parameterization used in this study is based on Eq. (1), which is a vector form of Eqs. (19) and (20) in Wu and Yanai (1994):

$$F_c = \sum_i \delta_i (\vec{v}_{Di} - \vec{v}) - M_c \frac{\partial \vec{v}}{\partial p} + \sum_i \gamma M_i \frac{\partial \vec{v}}{\partial p} \quad (1)$$

In Eq. (1), the subscript $()_i$ denotes each cloud element within the cloud ensemble, and an overbar $(\bar{\quad})$ denotes a gridcell-mean value. The parameters and variables in Eq. (1) are summarized in Table 1. Note that $M_c = \sum M_i$.

Cloud air is only partially mixed with environmental air as it rises, and so the detrained mass at the cloud top retains some memory of the lower-level momentum. The first term, in which the detrained mass flux at cloud top multiplies the momentum difference between the cloud and environment, represents a momentum transport from lower to upper levels. This term is significant only at upper levels where the cloud tops are located. The second and third terms dominate at lower levels. The second term, which represents the downward momentum transport by the environmental subsidence that compensates the convective mass flux, depends upon the magnitude of the convective mass flux and the environmental wind shear. Thus the first and second terms of Eq. (1) represent a “two-way” transport of momentum between upper and lower levels in the atmosphere, which communicate with each other via CMT in regions of strong vertical wind shear and convective activity.

The horizontal pressure gradient force produced by convective-scale pressure perturbations is expressed in the third term using the vertical wind shear, cloud mass flux,

Table 1 Descriptions for the parameters and variables in Eq. (1)

| | Description |
|------------|--|
| F_c | Momentum forcing by convective momentum transport |
| δ_i | Detrained mass flux by i th cumulus cloud |
| D_i | Wind inside the i th cumulus cloud at the detrainment (cloud top) level |
| \vec{v} | Environmental wind |
| M_c | Vertical mass flux produced by cumulus ensemble |
| M_i | Vertical mass flux produced by i th cumulus cloud |
| γ | Nondimensional constant representing the degree of organization for cumulus clouds |

and the orientation of organized clouds. From the shallow, inviscid, inelastic equations (Ogura and Phillips 1962), Rotunno and Klemp (1982) derived a relationship between the convective-scale pressure perturbation and the product of vertical wind shear and horizontal updraft variations. When an axisymmetric updraft occurs within vertical wind shear, a high (low) pressure perturbation is generated in the upshear (downshear) flank (see Fig. 3a of Rotunno and Klemp 1982). Wu and Yanai (1994) further assumed a sinusoidal pressure perturbation field and parameterized the pressure gradient force as the third term on the right hand side of Eq. (1). Here γ represents the orientation of organized convection with respect to the direction of the vertical wind shear. In reality, γ might depend on large scale variables (e.g., low level shear, Wu and Yanai 1994) and vary with space and time. For simplicity, we use a constant value of $\gamma = 0.55$, following Zhang and Wu (2003) who obtained this value as the best fit to the pressure gradient momentum forcing from their cloud resolving simulation. In Eq. (1), therefore, the second and third terms in Eq. (1) can be combined to yield

$$F_c = \sum_i \delta_i (\vec{v}_{Di} - \vec{v}) - (1 - \gamma) M_c \frac{\partial \vec{v}}{\partial p} \quad (2)$$

In Eq. (2), γ controls the magnitude of the third term (associated with subgrid pressure gradients) relative to the second term (vertical advection). When $\gamma < 1$ ($\gamma > 1$), the second (third) term dominates and CMT reduces (enhances) the vertical wind shear below the cloud top. Upgradient momentum forcing ($\gamma > 1$) is typically accompanied by a squall line (Wu and Yanai 1994). Figure 1 is a schematic diagram of the above, for an idealized convective grid cell with vertical wind shear. Solid and dashed lines represent environmental (\bar{u}) and in-cloud (u_c) vertical wind structure, respectively, which differ within the cloud layer. A convective-scale pressure perturbation (p') is also drawn (dotted line). Three kinds of mass fluxes—updrafts (M_c), detrainment, and subsidence—are expressed by arrows. The numbers show the region where each term of Eq. (1) is active. The first term is active at cloud top, where there is detrainment mass flux and the environmental and in-cloud momentum differ. The second and third terms play roles at almost all levels between the cloud bottom and top, with their magnitude depending on the magnitude of the vertical wind shear and vertical mass flux. Note that the third term, which represents interactions between convective-scale pressure perturbations and environmental wind shear, is parameterized using the vertical mass flux and environmental wind shear.

To implement the scheme in the SNU AGCM, the vertical mass flux and detrained mass at cloud top are obtained from the original convection scheme (Numaguti

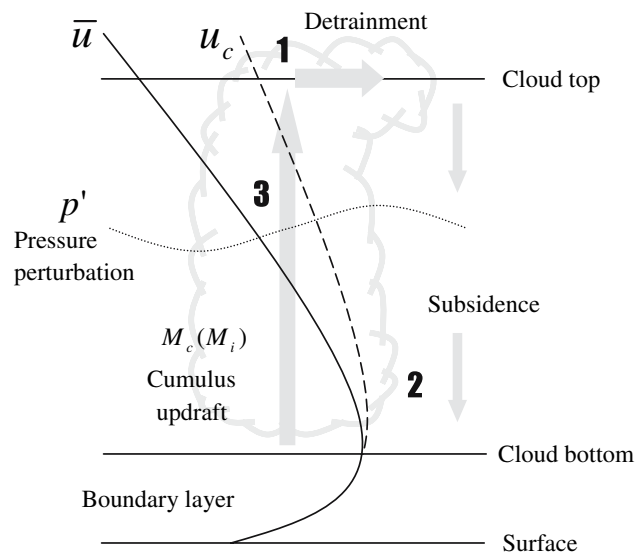


Fig. 1 Schematic diagram of an idealized convective grid cell with vertical wind shear. Solid and dashed lines represent environmental and in-cloud vertical wind structure, respectively. The convective scale pressure perturbation is also drawn (dotted line). Arrows represent mass fluxes. Numbers indicate the region where each term of Eq. (1) is active. See text for details

et al. 1995). The vertical wind profile inside the cumulus clouds is calculated from the momentum budget equations using Eqs. (24)–(27) of Wu and Yanai (1994).

2.2 Model and experimental design

The models used in this study are the Seoul National University atmospheric general circulation model (SNU AGCM) and SNU coupled GCM (SNU CGCM). The SNU AGCM is a global spectral model at T42 resolution, with 20 vertical sigma levels. The deep convection scheme is a simplified version of the relaxed Arakawa-Schubert scheme (SAS, Numaguti et al. 1995). The large-scale condensation scheme consists of a prognostic microphysics parameterization for total cloud liquid water (Le Treut and Li 1991) with a diagnostic cloud fraction parameterization. A non-precipitating shallow convection scheme (Tiedtke 1983) is also implemented in the model for the mid-tropospheric moist convection. The boundary layer scheme is a non-local diffusion scheme based on Holtslag and Boville (1993), while the land surface model is from Bonan (1996). Atmospheric radiation is parameterized by a two-stream k distribution scheme as in Nakajima et al. (1995). Other details of the model physics are described in Lee et al. (2001, 2003).

To examine the impact of CMT on the ENSO simulation, the AGCM is integrated with perpetual solar conditions corresponding to the 16th of January, with either

climatological DJF SST or El Niño-like DJF SST as boundary conditions. The El Niño SST is constructed from the five strongest observed El Niño and La Niña events, based on DJF NINO3.4 SSTs over 1950–2003. Those events are 1957/1958, 1972/1973, 1982/1983, 1991/1992 and 1997/1998 for El Niño and 1973/1974, 1975/1976, 1988/1989, 1998/1999 and 1999/2000 for La Niña. We use the symmetric part of the SST anomaly (Fig. 2) by taking the average El Niño SST minus the average La Niña SST, all divided by 2. The SST anomalies are superposed on the climatological SST over the Pacific region (120°E–85°W, 20°S–20°N); elsewhere climatological SST is prescribed. Four experiments are carried out, with two SST boundary conditions and two versions of the AGCM with or without CMT parameterization. The AGCM is integrated for 1 year in each experiment. The first 50 days of simulation are discarded to avoid artifacts of initialization, and the remainder is used in this study. Hereafter, the AGCM simulations with/without CMT parameterization are referred to as CTLa and CMTa, respectively.

The CGCM used in this study was developed at Seoul National University. It couples the above AGCM to the oceanic GCM developed at the Geophysical Fluid Dynamics Laboratory (GFDL). The ocean model—MOM2.2—is a B-grid finite difference treatment of the primitive equations of motion, using the Boussinesq and hydrostatic approximations in spherical coordinates, and covers the global oceans with realistic coastlines and bottom topography. The zonal grid spacing is 1.0°. The meridional grid spacing between 8°S and 8°N is 1/3°, gradually increasing to 3.0° at 30°S and 30°N, and is fixed at 3.0° in the extratropics. There are 32 vertical levels with 23 levels in the upper 450 m. A mixed layer model, developed by Noh and Kim (1999) is embedded into the ocean model to improve the climatological vertical structure of the upper ocean.

The ocean model communicates once per day with the atmospheric model, exchanging SST, wind stress, freshwater flux, longwave and shortwave radiation, and turbulent fluxes of sensible and latent heat. No flux correction is applied, and the model does not exhibit significant climate drift in long-term simulations. In

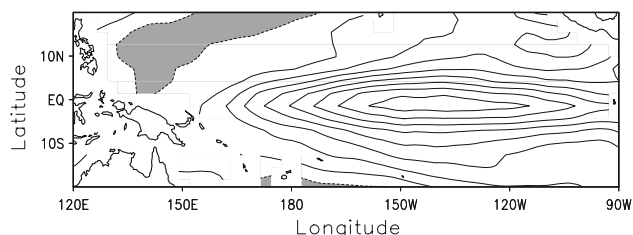


Fig. 2 Idealized El Niño SST anomaly for DJF. Contour interval is 0.3°C. Dashed line represents negative values

addition, the CGCM reasonably simulates the observed climatology and ENSO, though some systematic biases are found (Kug et al. 2007b). Hereafter, the CGCM simulation without the CMT parameterization is referred to as CTLc and integrated for 200 years. The CGCM simulation with CMT is referred to as CMTc and is integrated for 50 years.

2.3 Observational data

For observed rainfall we use the 1979–2003 monthly mean data from the Climate Prediction Center (CPC) Merged Analysis of Precipitation (CMAP, Xie and Arkin 1997). Monthly-mean winds are from the National Centers for Environmental Prediction/National Center for Atmospheric Research reanalysis (NCEP/NCAR, Kalnay et al. 1996), and wind stress data is from the European Centre for Medium-Range Weather Forecasts (ECMWF) 40-year reanalysis (ERA40, Uppala et al. 2005). SSTs are from the National Oceanic and Atmospheric Administration (NOAA) Extended Reconstructed Sea Surface Temperatures (ERSST, Smith and Reynolds 2004).

3 AGCM experiments

3.1 Climatology simulation

To set the stage for the perpetual El Niño simulations, we first examine the atmospheric response to perpetual climatological DJF SST. We shall refer to the time-averaged simulated fields from this run as the “DJF climatology”. Vertical wind shear, defined as the zonal wind at 850 hPa minus that at 200 hPa (Fig. 3) and precipitation (Fig. 5) are compared with observations. One might expect CMT to affect the climatological wind shear by mixing momentum between the upper and lower levels. Note that the second term in Eq. (1) depends on both the magnitude and the sign of the vertical wind shear.

Observed and simulated DJF mean vertical wind shears are shown in Fig. 3. In the observations, the Walker Circulation produces westerly shear over most of the tropical Pacific, while easterly shear covers the western equatorial Pacific from the maritime continent to the date line (Fig. 3a). Both the CTLa (Fig. 3b) and CMTa (Fig. 3c) reasonably capture these features. The easterly shear in the CTLa; however, extends only to 160°E. CMTa reproduces the observed eastward extension of the easterly shear to 180°E, but the magnitude of easterly shear is larger in CMTa than in CTLa and NCEP.

By construction, the parameterized CMT should act like diffusion, reducing the local vertical wind shear. The CMT-induced increase of easterly wind shear in the

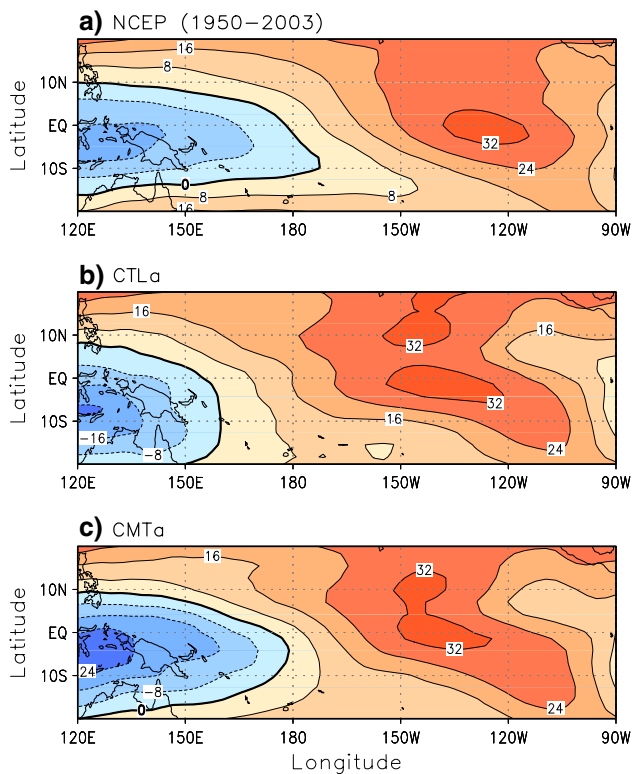


Fig. 3 DJF mean vertical wind shear over the tropical Pacific. Units are m/s. **a** NCEP, **b** CTLα and **c** CMTα

western Pacific is related to changes in the low level circulation and precipitation (as discussed later), and also to the basic vertical structure of the zonal wind, shown for CTLα in Fig. 4. CTLα simulates a westerly peak in climatological wind shear at 600 hPa in the western Pacific, so adding CMT spreads westerly momentum down to 850 hPa. Similarly, adding CMT spreads easterly momentum from the easterly peak at 100 hPa down to 200 hPa. Both act to increase the easterly wind shear between 850 and 200 hPa. Compared to CTLα, CMTα has substantially smaller root mean square errors (RMSEs), and stronger pattern correlations with observations, for climatological rainfall and wind shear over the tropical Pacific (120°E–90°W, 20°S–20°N) and the global as a whole (Table 2). The 850 hPa zonal wind is also closer to observation in CMTα than CTLα (not shown). That CMT improves the simulated mean winds, especially in the tropics, is consistent with previous studies (Tiedtke 1989; Zhang and McFarlane, 1995; Gregory et al. 1997).

Figure 5 shows the observed and AGCM-simulated DJF mean precipitation. In observations, the SPCZ extends from the western Pacific to the southern central Pacific, and precipitation is relatively weak near the equator. The two AGCMs capture those overall characteristics but have different precipitation biases. CTLα (Fig. 5b) underestimates the rainfall in the SPCZ and overestimates it near the

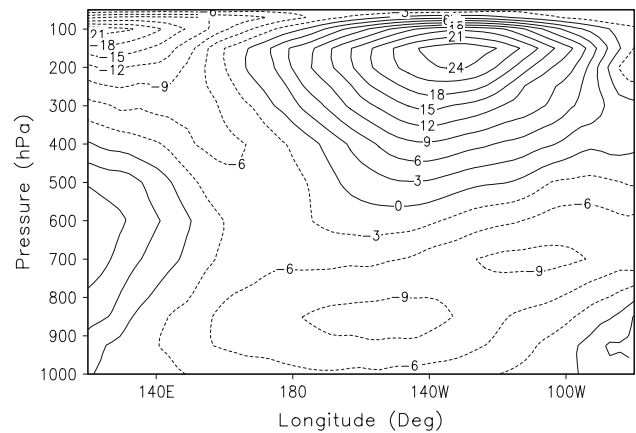


Fig. 4 Longitude-height diagram of 5N–5S averaged zonal wind in the Pacific for DJF. Contour interval is 3 m s^{-1} . Dashed line represents negative values

equator. CMTα (Fig. 5c) exhibits less rain near the equator and more off-equator, resulting in a more clearly-separated ITCZ and SPCZ. Note that Wu et al. (2003) also showed reduced DJF precipitation in the equatorial western Pacific upon inclusion of CMT in their model (their Fig. 3). The distinct differences between the present two cases indicate that the CMT parameterization has a significant impact on the simulation of tropical precipitation (Fig. 6b), leading to a more realistic pattern of DJF climatological rainfall in terms of both RMSE and pattern correlation with observations (Table 2).

The reduction (increase) of precipitation in equatorial (off-equatorial) regions may be related to the meridional divergent circulation at low levels. In CMTα, the meridional circulation is reduced near the equator, implying a weaker local Hadley circulation due to enhanced mixing between the lower inflow and upper outflow. These results are consistent with those of Wu et al. (2007), who analyzed the impact of the CMT parameterization in a different AGCM.

Table 2 Root mean squared errors (RMSE) and pattern correlations between AGCM simulated DJF climatological field and observation

| | RMSE | | Pattern correlation | |
|-----------------------|---------|--------|---------------------|--------|
| | Pacific | Global | Pacific | Global |
| SHEAR (Fig. 2) | | | | |
| CTL | 8.01 | 5.87 | 0.85 | 0.91 |
| CMT | 5.51 | 4.99 | 0.94 | 0.94 |
| PRCP (Fig. 3) | | | | |
| CTL | 3.73 | 2.23 | 0.60 | 0.69 |
| CMT | 2.73 | 1.86 | 0.78 | 0.77 |

Units of RMSE are m/s for shear, mm/day for precipitation. See the text for details

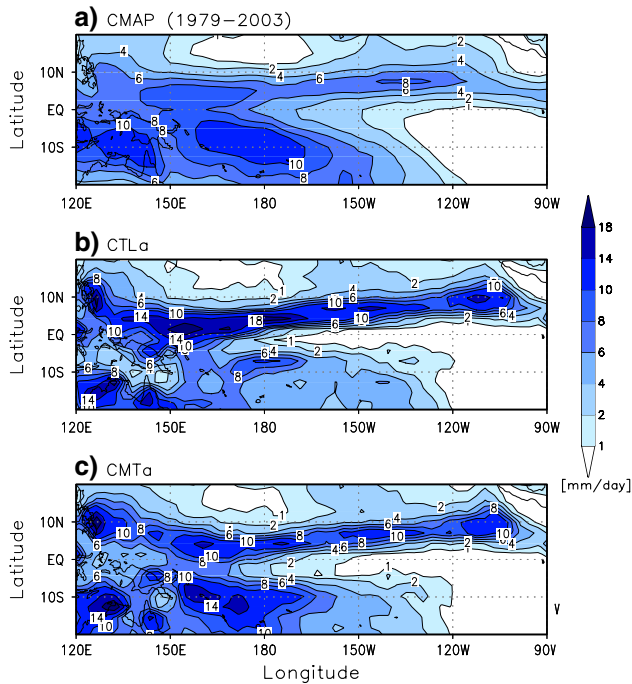


Fig. 5 DJF mean precipitation over the tropical Pacific. Units are mm day^{-1} . **a** CMAP, **b** CTL α and **c** CMT α

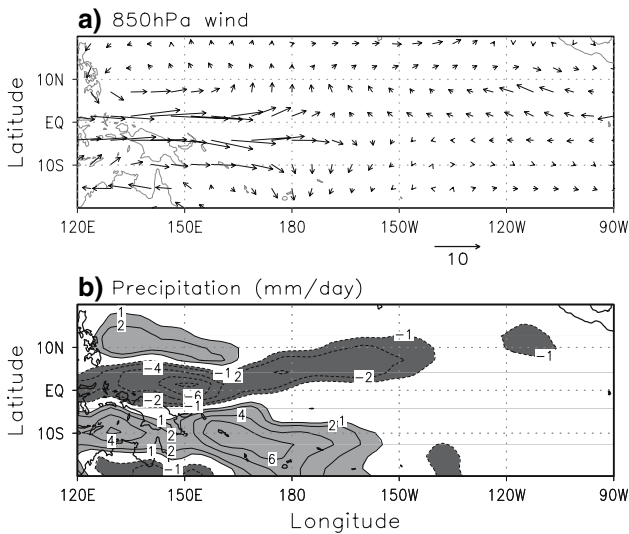


Fig. 6 **a** 850 hPa zonal wind difference between CMT α and CTL α in the DJF climatological SST simulation. **b** Same as **a**, except for precipitation

The difference in precipitation (Fig. 6b) between CMT α and CTL α is related to changes in low level circulation (Fig. 6a). Over the warm pool in CTL α , the climatological low level vertical shear is westerly (due to a westerly wind maximum at 600 hPa, Fig. 4), so that CMT induces westerly momentum forcing at low levels. Increased precipitation off-equator also induces low level westerlies

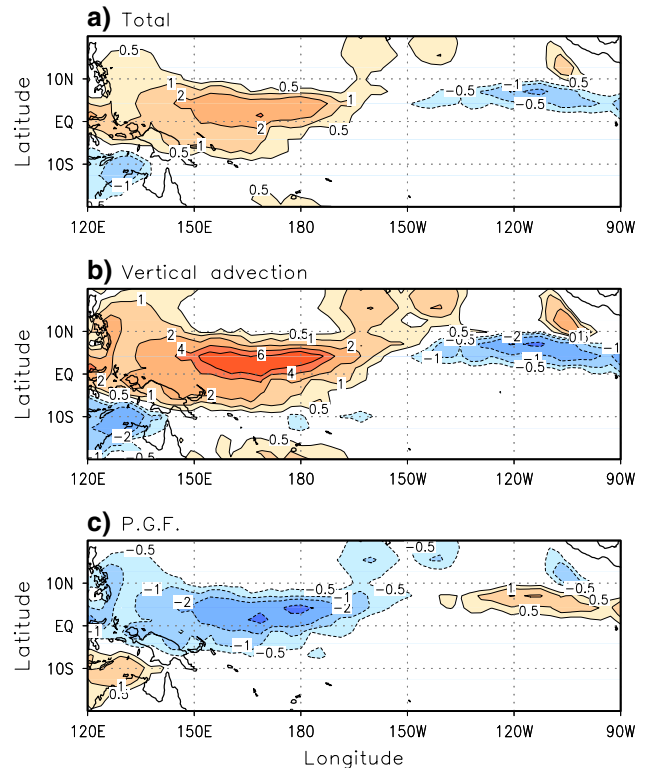


Fig. 7 DJF mean momentum forcing at 850 hPa level from CMT α with climatological SST. **a** Total, **b** vertical advection and **c** pressure gradient force. Units are $\text{m s}^{-1} \text{day}^{-1}$

via the Gill-type response to off-equatorial atmospheric heating. Due to these two effects, CMT α simulates stronger low-level westerlies over the western Pacific than does CTL α (Fig. 6a).

To understand how CMT alters the climatological wind, we compute a momentum budget following Eq. (1). Figure 7a shows that the momentum forcing by CMT accounts for most of the enhanced westerlies. Figure 7 also shows the vertical advection (Fig. 7b) and pressure gradient force (Fig. 7c) terms in Eq. (1). The first term of Eq. (1) is not shown, because it is relatively small at low levels where cloud tops seldom form. As mentioned before, the pressure gradient force term has similar pattern to vertical advection term but has opposite sign with smaller—about half—value. Vertical advection is important in the northern ITCZ, where convective mass flux is strong relative to precipitation (Fig. 5c).

3.2 El Nino anomaly simulation

In the previous section, we showed that the CMT parameterization has large impacts on the climatological simulation by changing momentum budget. Next we examine the impact of CMT on the atmospheric response

to El Nino SST forcing, by subtracting the climatological SST runs from the El Nino SST runs described in Sect. 2. Figure 8 shows the anomalous precipitation associated with El Nino in CMAP, CMTa and CTLa. The El Nino anomaly for CMAP is obtained by compositing the DJF anomalies from the three largest observed El Ninos (1982/1983, 1991/1992 and 1997/1998). In CMAP (Fig. 8a), a positive (negative) rainfall anomaly appears in the central (western) Pacific. Both CTLa (Fig. 8b) and CMTa (Fig. 8c) fail to capture the negative anomaly over the Maritime continent, although the negative anomaly in the western North Pacific region is well produced in both simulations. The positive anomalies in both simulations are shifted to the west by about 20 degrees compared to the CMAP. While the systematic biases of precipitation are similar in the two simulations, close examination of Fig. 8 reveals that the equatorial rainfall anomaly is meridionally wider and shifted a bit farther east in CMTa than in CTLa.

Figure 9 shows zonal wind anomalies at 850 hPa, which is generally above cloud base. Momentum forcing by CMT at 850 hPa is readily transmitted to the surface via the vertical diffusion/PBL scheme. During the observed El Nino, strong anomalous westerlies appear east of the date line (Fig. 9a). Both CTLa and CMTa displace these westerly anomalies westward by about 20 degrees relative to the observed patterns, consistent with the bias in

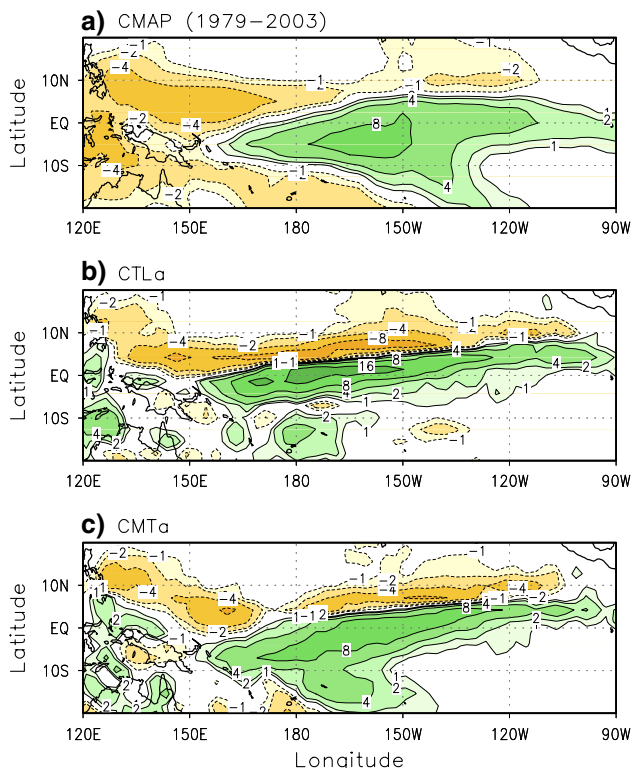


Fig. 8 ENSO anomalies of precipitation. **a** CMAP, **b** CTLa and **c** CMTa. Units are mm day^{-1}

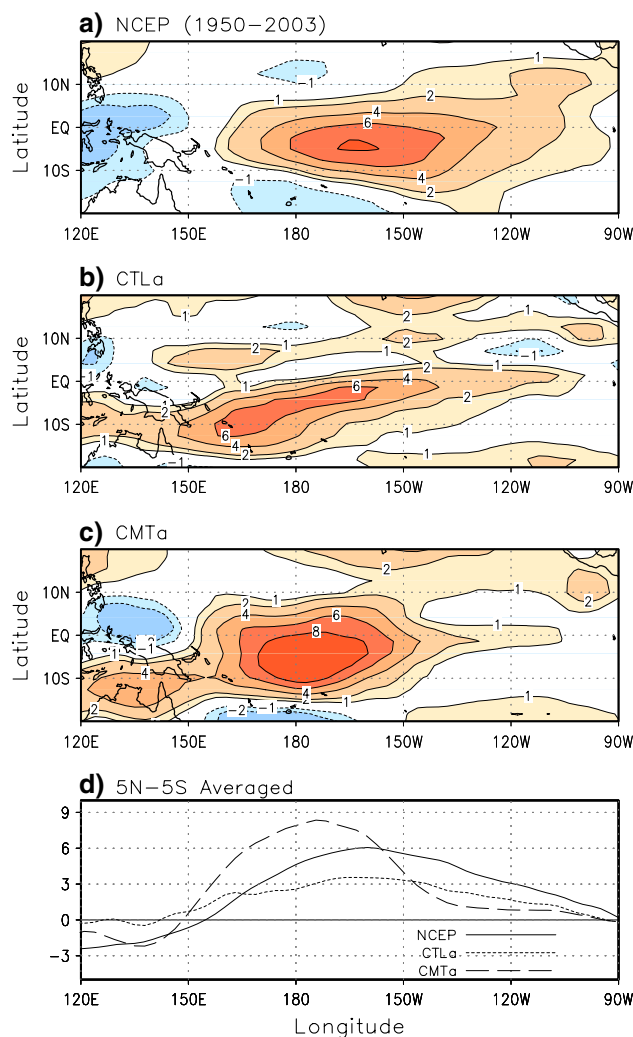


Fig. 9 ENSO anomalies of 850 hPa zonal wind. **a** NCEP, **b** CTLa and **c** CMTa. **d** 5N-5S averaged anomalies. Units are m s^{-1}

precipitation anomalies (Fig. 8). Yet despite the very similar-looking precipitation patterns between the two models, their wind anomaly patterns are quite different—indicating that CMT induces a significant change in winds despite similar atmospheric heating. Compared to CTLa, CMTa shows a zonal wind response (Fig. 9c) which is better organized, and exhibits stronger, meridionally broader, and more equatorially-centered anomalous westerlies that better resemble observations. The pattern correlation with the observed zonal wind field is 0.41 for CTLa, 0.58 for CMTa. The CMT-induced doubling in the strength of the anomalous westerly response to El Nino SSTAs (Fig. 9d) would likely produce a greater impact on the ocean in a coupled model.

The CMT-induced difference in the El Nino 850 hPa zonal wind anomaly (Fig. 10a) clearly shows the larger westerlies in CMTa over the central Pacific. This wind difference is largely attributable to local momentum

forcing from CMT, which has a very similar pattern (Fig. 10b). During El Nino the centers of convection in the western Pacific expand eastward toward the central Pacific (Kidson 1975; Saravanan and Chang 2000; Ham et al. 2007), enhancing the CMT over the central Pacific and producing a stronger anomalous westerly wind response.

3.3 Momentum budget for the El Nino westerly wind anomaly in CMTa

Next we examine how CMT enhances the El Nino westerly wind anomaly, by analyzing the individual terms in Eq. (1). The dominant contribution is from vertical advection (Fig. 10c), which is a product of the environmental wind shear and convective mass flux. Decomposing the daily-mean data into climatological mean, seasonal mean anomaly and daily transients the anomalous vertical advection term becomes:

$$\begin{aligned}
 -\overline{M_c^E} \frac{\partial u^E}{\partial p} + \overline{M_c^C} \frac{\partial u^C}{\partial p} = & \left[-\overline{(M_c^E)} \frac{\partial}{\partial p} (u^E)' \right]_A \\
 & + \left[-(M_c^E)' \frac{\partial}{\partial p} u^C \right]_B \\
 & + \left[-(M_c^E)' \frac{\partial}{\partial p} (u^E)' \right]_C \\
 & + \left[-\overline{(M_c^E)''} \frac{\partial}{\partial p} (u^E)'' + \overline{(M_c^C)''} \frac{\partial}{\partial p} (u^C)'' \right]_D
 \end{aligned} \tag{3}$$

where brackets and subscripts identify the terms shown in Fig. 11 and discussed below. (Details may be found in the Appendix .) Note that the sum of these bracketed terms (Fig. 11a) is nearly the same as the total vertical advection term (Fig. 10c) in terms of pattern and magnitude.

Term A plays a significant role in the northern ITCZ (Fig. 11b). The largest contribution in the central Pacific is from term B, which consists of vertical advection by the seasonally anomalous mass flux acting on the climatological wind shear (Fig. 11c). In particular, the central Pacific anomalous westerlies in Fig. 10a are the result of anomalous environmental subsidence (which compensates the anomalous convective mass flux) acting on the local climatological westerly wind shear, conveying westerly momentum downward to low levels.

The second largest term in the central Pacific region is term C. Because this term is a nonlinear product of the anomalous mass flux and anomalous wind shear, it can contribute to an asymmetric zonal wind anomaly response between El Nino and La Nina (cf. Kang and Kug 2002). Interestingly, term C actually *enhances* the low-level westerly forcing in the central Pacific from term B. This is rather counterintuitive, as one might have expected that

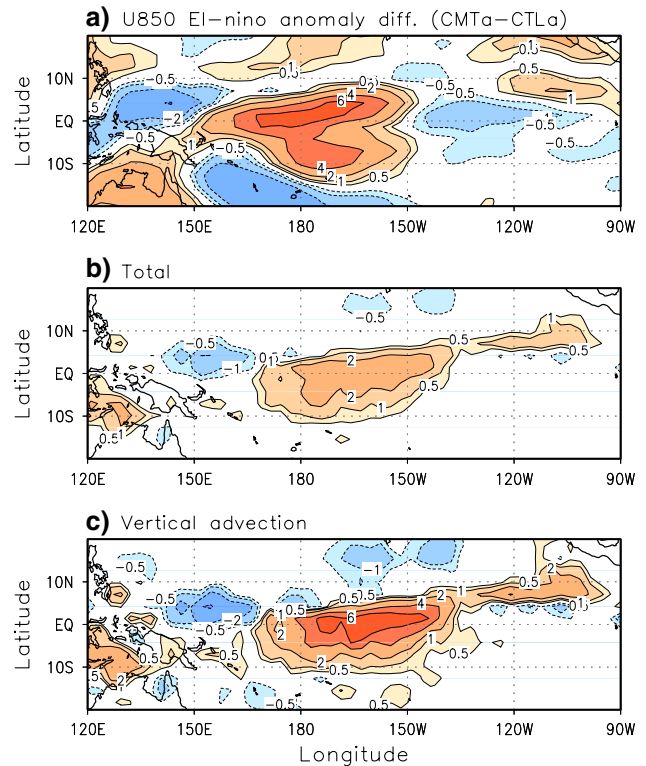
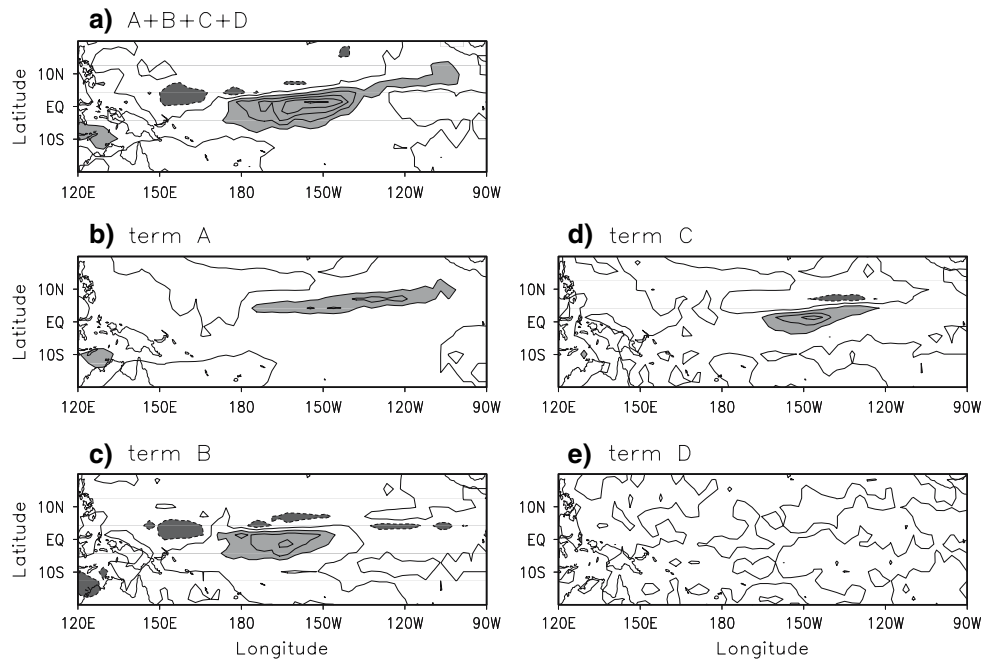


Fig. 10 a Difference in ENSO 850 hpa zonal wind anomalies between CMTa and CTLa. Units are $m s^{-1}$. El Nino momentum forcing anomaly from b total of all terms, c vertical advection only. Units are $m s^{-1} day^{-1}$

during El Nino, a weakening Walker cell would have *reduced* the westerly vertical wind shear and therefore the ability of anomalous convection (and its associated environmental subsidence) to convey mid-tropospheric westerly momentum downward into the PBL. However, a vertical section of the zonal wind anomalies along the equator (not shown) reveals that in CMTa the peak El Nino westerly anomaly—associated with the weakening Walker cell—sits well above the boundary layer, between 850 and 700 hPa. This anomalous westerly momentum is conveyed down into the PBL via the anomalously strong convection during El Nino, so that term C aids term B in driving the surface westerly anomalies. We performed the same calculation using the results from CTLa, which can be viewed as a run in which interactions between CMT and the atmospheric circulation are suppressed. The sum of the four terms on the right hand side of Eq. (3), and term B alone, are both smaller for CTLa than for CMTa (not shown). In addition, in CTLa term C has a sign opposite that of term B (and term C in CMTa), and largely cancels term B over the central Pacific—so that term A dominates the gross pattern of central Pacific anomalous momentum forcing in CTLa. From comparison of the CTLa and CMTa momentum budgets, it is thus apparent that the CMT-

Fig. 11 Vertical advection terms in the CMT parameterization, decomposed as in the Appendix. Contour interval is $1.5 \text{ ms}^{-1} \text{ day}^{-1}$. **a** Total, **b** term A, **c** term B, **d** term C and **e** term D. See text for details



induced changes in large-scale circulation enhance the direct effects of CMT, by feeding back through the changes in climatological and anomalous wind shear and the distribution of convective activity.

4 CGCM simulation

To assess the impact of CMT in coupled simulations, we compared simulations of the SNU coupled GCM with/without the CMT parameterization (CTLc/CMTc). CTLc was integrated for 200 years, CMTc for 50 years. Figure 12 shows the DJF-mean climatological biases of SST, precipitation, and zonal wind stress in the two simulations. CTLc exhibits a strong cold bias over the central Pacific, common problem of state-of-art coupled GCMs (Latif et al. 2003). CTLc also has too little precipitation and wind convergence in the western Pacific, with an equatorial easterly wind bias in the western Pacific and a westerly wind bias in the central Pacific. CMTc shows a reduction in all of these biases, with more rain and additional low-level westerlies in the west Pacific (as also seen in the AGCM simulations), and a $\sim 1^\circ\text{C}$ warming of the central equatorial Pacific.

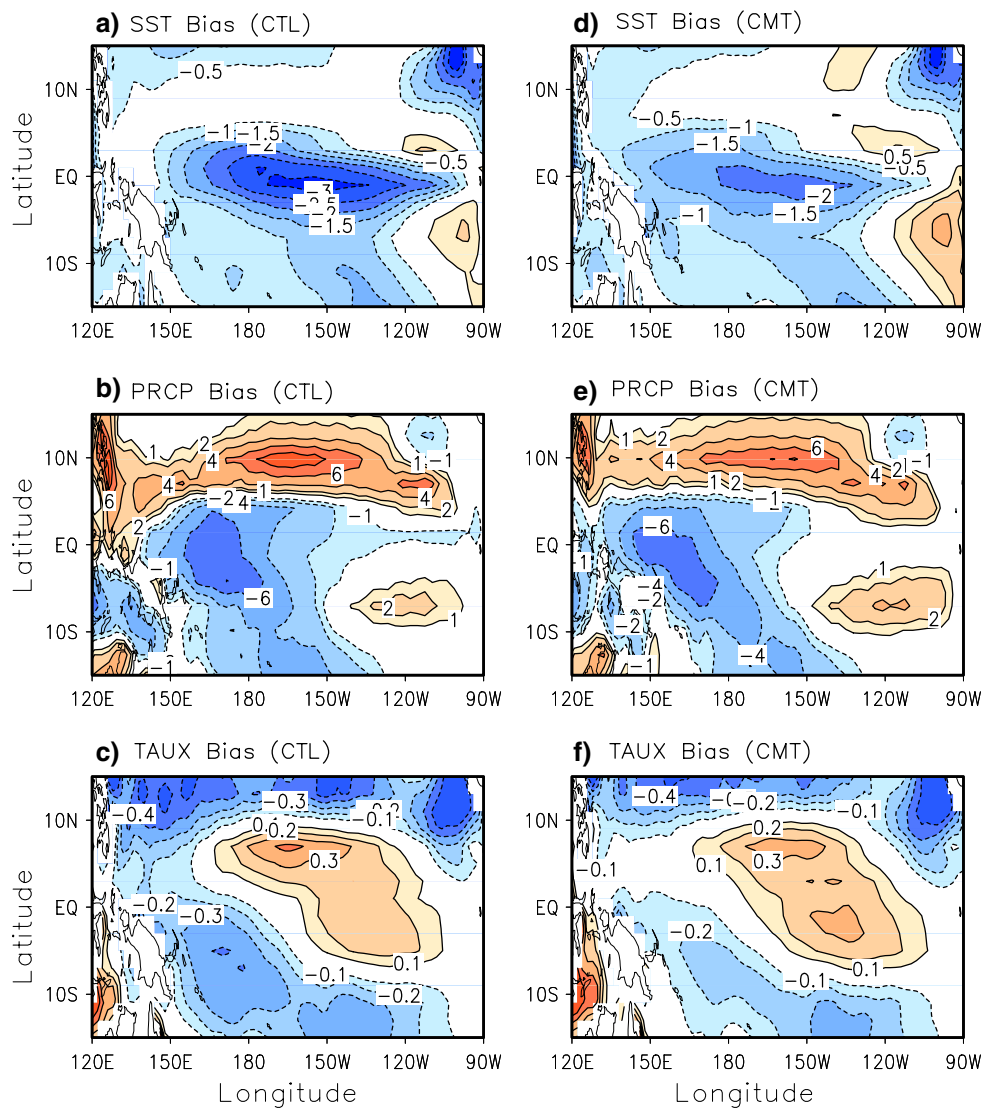
Based on the results presented thus far, one could expect CMT to alter the behavior of ENSO in the CGCM. Many studies (e.g., Fedorov and Philander 2001; Wittenberg 2002; and references therein) have shown ENSO to be sensitive to changes in the background state, while others (Kirtman 1997; An and Wang 2000; Capotondi et al. 2006) have shown ENSO to be sensitive to changes in the

anomalous atmospheric response to SSTAs, like those seen in Sect. 3.

As a measure of ENSO amplitude, we compute the standard deviation of NINO3.4 SST anomalies. Compared to the observed amplitude of 0.90°C , CTLc is a bit too weak (0.70°C). But CMTc is much stronger (1.46°C)—consistent with the stronger equatorial wind stress response of the atmosphere model with CMT (Sect. 3.2), and also with the reduced equatorial cold bias in the coupled model, which promotes eastward shifts of convection (Kug et al. 2007a). Figure 13 shows the SST pattern associated with El Niño, obtained by regressing the SST anomalies for all months onto NINO3.4, and then multiplying by the standard deviation of NINO3.4. The observed SST anomalies are largest along the equator in central and eastern Pacific, with a peak near 150°W (Fig. 13a). CTLc and CMTc display a very similar pattern, despite their substantial differences in amplitude.

Figure 14 shows regressions of precipitation and wind stress anomalies onto DJF NINO3.4 SSTA, multiplied by the standard deviation of NINO3.4 as in Fig. 13. The observed ENSO precipitation anomaly is positive (negative) in the central (western) Pacific (Fig. 14a), and is accompanied by westerly wind stress anomalies in central Pacific. In CTLc (Fig. 14b), the positive precipitation anomaly is weaker than observed, and its longitudinal position is shifted about 30 degrees too far west—both common problems in state-of-the-art coupled GCMs, which have cold biases over the central Pacific (Mechoso et al. 1995). The CTLc westerly wind stress anomaly is also weaker than observed. However, CMTc (Fig. 14c)

Fig. 12 Biases of the coupled model simulations. *Right panels* are for the control experiment, *left panels* are for the experiment with CMT. **a** and **d** SST; **b** and **e** precipitation; **c** and **f** wind stress



enhances the positive precipitation anomaly and shifts it eastward. In both models there are two (northern and southern) precipitation maxima (presumably related to the climatological double ITCZ), with the westerly wind stress signal clearest along the southern precipitation peak.

Unlike the AGCM results in Sect. 3.2, the coupled precipitation anomaly pattern changes substantially when CMT is added. We hypothesize that these changes are linked to the reduced cold bias in CMTc, which promotes greater eastward shifts of convection during ENSO warm events. In addition, this better placement of the atmospheric heat source when CMT is added could help improve the simulation of ENSO teleconnections around the globe. When CMT is added, the ENSO wind stress response changes—not only in magnitude but in longitudinal location and meridional width. In intermediate-complexity models, an eastward shift and meridional widening of the zonal wind stress tends to produce longer-

period ENSOs, by slowing the oceanic adjustment via oceanic Rossby waves (Cane et al. 1990; Kirtman 1997; An and Wang 2000; Kang and Kug 2002; Kug et al. 2003). This was recently confirmed for state-of-the-art CGCMs by Capotondi et al. (2006), who found that the period of the IPCC AR4 models could largely be predicted from knowing only the meridional width and central longitude of the anomalous westerly wind stress response during El Niño. The impact of CMT on the ENSO time scale of the SNU CGCM is illustrated in Fig. 15. Although both CTLc and CMTc show a narrower NINO3.4 SSTA autocorrelation function (and thus a shorter period) than observed, CMTc does have a relatively broader autocorrelation function—implying a longer and more realistic ENSO time scale. This is consistent with what would have been expected from previous studies, based on the eastward shift and meridional widening of the anomalous zonal wind stress response when CMT was added.

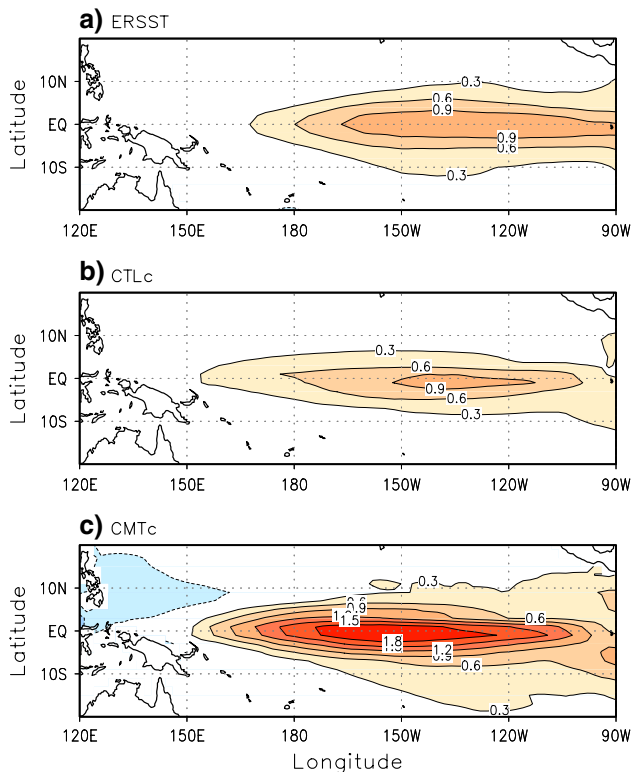


Fig. 13 SST regressed onto the Niño 3.4 index, and then multiplied by the standard deviation of the Niño 3.4 index. Contour interval is 0.3 and units are °C. All months are used in the calculation. **a** ERSST, **b** CTLc and **c** CMTc

5 Summary and discussion

The impact of convective momentum transport (CMT) on the simulation of the tropical Pacific climatology and ENSO response were investigated using AGCM integrations and multi-decadal coupled model integrations. We parameterize the CMT in both GCMs following the method of Wu and Yanai (1994). In our CMT formulation, the pressure gradient force is expressed in terms of the vertical wind shear, convective mass flux, and the orientation of organized convection, with the latter fixed at a constant value derived from a fit to a cloud resolving model.

Adding CMT to the AGCM improves the climatological mean fields of precipitation and 850 hPa zonal wind. Among the three terms that constitute momentum forcing by the CMT, vertical advection dominates at low levels. The El Niño anomaly patterns of precipitation and 850 hPa zonal wind, which represent the atmospheric feedbacks to the ocean, are also affected and more closely resemble the observed patterns when CMT is included. The CMT leads to stronger and better organized low level westerly wind anomalies near the equator, and widens them meridionally. The most important factor for these differences is the anomalous convective mass flux, which is associated with

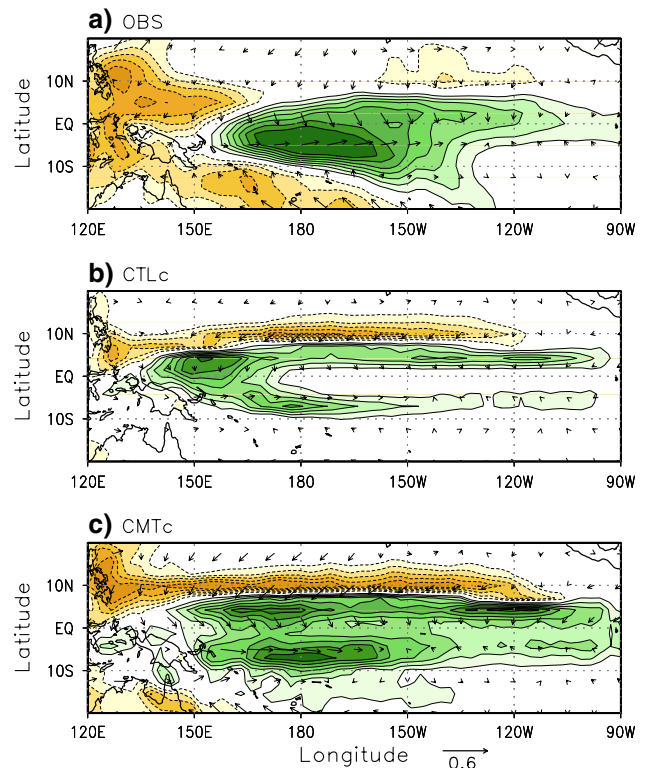


Fig. 14 Precipitation (shaded) and wind stress (vectors) regressed onto the Niño 3.4 index, and then multiplied by the standard deviation of the Niño 3.4 index. Only DJF months are used. Contour interval is 0.5 and zero lines are not drawn. **a** OBS, **b** CTLc and **c** CMTc

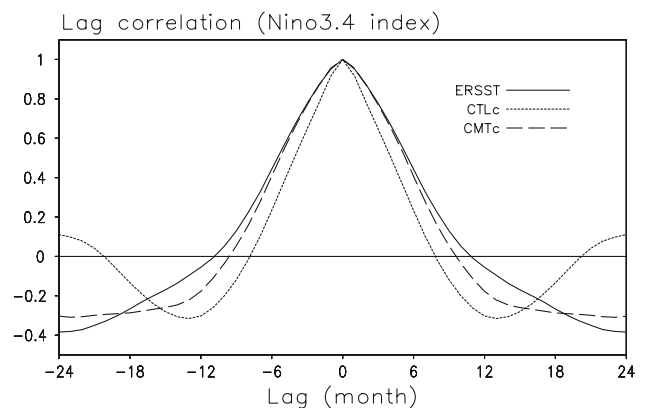


Fig. 15 Temporal autocorrelation of the Niño 3.4 index for ERSST (solid), CMTc (dashed) and CTLc (dotted)

the eastward shift of convection from the western to the central Pacific region during El Niño.

Similar results are obtained from multi-decadal simulations of the SNU coupled model. With CMT, the climatological biases of SST, precipitation and wind stress are reduced. ENSO SST variability is amplified, with stronger precipitation and wind anomalies over the central Pacific. The ENSO period, which is sensitive to the zonal position and meridional width of the westerly wind stress

anomalies, grows longer and closer to observations when CMT is added.

Interestingly, in contrast to the control run which had slightly weaker amplitude than observations, adding CMT results in excessive ENSO SST variance, despite the wind stress anomalies having a magnitude comparable to observations. This implies that some processes may be exaggerating the ENSO SST anomalies. Absence of diurnal variation is one possible candidate. From other experiments, we have found the ENSO amplitude to be significantly reduced when the atmosphere/ocean coupling interval is reduced from 1 day to 3 h (not shown). Further study is needed to understand these sensitivities.

We have shown that CMT can have a large impact on an ENSO simulation. It is possible that CMT may also have significant impacts on other climate phenomena like the MJO and monsoons, either directly by changing the atmospheric response to convection, or indirectly by altering the background climatology and ENSO. In fact, we have found the intraseasonal (20–100 day) variability to be greatly enhanced in the equatorial Pacific when CMT is added (not shown), possibly due to enhanced easterly shear over the western Pacific. However, further studies will be required to determine how CMT affects the relatively shorter-term atmospheric variability.

Acknowledgments The work was supported by the SRC program of Korea Science and Engineering Foundation, and Brain Korea 21 Project. I.-S. Kang was supported by Ministry of Environment as “The Ecotechnopia 21 project”. F.-F. Jin was partly supported by NSF grants ATM-0652145 and ATM-0650552 and NOAA grants GC01-229.

6 Appendix

Budget calculation for anomalous vertical advection

Here, we derive Eq. (2) using daily averaged convective mass flux (M_c) and zonal wind (u). First the daily-mean variables from the climatological run ($(\)^C$) and El Nino SST run ($(\)^E$) are divided as follows,

$$\begin{aligned} M_c^C &= \overline{M_c^C} + (M_c^C)'' \\ u_c^C &= \overline{u_c^C} + (u_c^C)'' \end{aligned} \tag{1a}$$

$$\begin{aligned} M_c^E &= \overline{M_c^E} + (M_c^E)' + (M_c^E)'' \\ u_c^E &= \overline{u_c^E} + (u_c^E)' + (u_c^E)'' \end{aligned} \tag{2a}$$

where an overbar ($\overline{\ }$) denotes a seasonal mean value. A prime ($'$) denotes a seasonal-mean anomaly, and a double prime ($''$) a daily fluctuation. Note that the seasonal mean from the El Nino SST run is decomposed into a climatology and seasonal mean anomaly.

The vertical advection term in Eq. (1) is

$$-M_c \frac{\partial u}{\partial p} \tag{3a}$$

Substituting Eqs. (1a) and (2a) into (3a) and taking a seasonal mean, we get the seasonal mean momentum forcing by the CMT vertical advection term in Eq. (1).

For the climatology run,

$$-M_c^C \frac{\partial u^C}{\partial p} = -\overline{(M_c^C)} \frac{\partial \overline{u^C}}{\partial p} - \overline{(M_c^C)''} \frac{\partial (u^C)''}{\partial p} \tag{4a}$$

and for the El Nino SST run,

$$\begin{aligned} -M_c^E \frac{\partial u^E}{\partial p} &= -\overline{(M_c^E)} \frac{\partial \overline{u^E}}{\partial p} - \overline{(M_c^E)'} \frac{\partial (u^E)'}{\partial p} - \overline{(M_c^E)''} \frac{\partial u^E}{\partial p} \\ &\quad - (M_c^E)' \frac{\partial \overline{u^E}}{\partial p} - \overline{(M_c^E)''} \frac{\partial (u^E)''}{\partial p} \end{aligned} \tag{5a}$$

We then obtain the seasonally anomalous momentum forcing due to the CMT vertical advection term, by subtracting (5a) from (4a):

$$\begin{aligned} -M_c^E \frac{\partial u^E}{\partial p} + M_c^C \frac{\partial u^C}{\partial p} &= -\overline{(M_c^E)'} \frac{\partial (u^E)'}{\partial p} - \overline{(M_c^E)''} \frac{\partial u^E}{\partial p} \\ &\quad - (M_c^E)' \frac{\partial \overline{u^E}}{\partial p} - \overline{(M_c^E)''} \frac{\partial (u^E)''}{\partial p} \\ &\quad + \overline{(M_c^C)''} \frac{\partial (u^C)''}{\partial p} \end{aligned} \tag{6a}$$

Equation (6a) is repeated in the main text as Eq. (2). We label the four terms in the right hand side of Eq. (6a) as follows:

Term A—climatological mass flux and seasonally anomalous wind shear

$$-\overline{(M_c^C)''} \frac{\partial (u^C)''}{\partial p} \tag{7a}$$

Term B—seasonally anomalous mass flux and climatological wind shear

$$-(M_c^E)' \frac{\partial \overline{u^E}}{\partial p} \tag{8a}$$

Term C—seasonally anomalous mass flux and seasonally anomalous wind shear

$$-(M_c^E)' \frac{\partial (u^E)'}{\partial p} \tag{9a}$$

Term D—change in transient eddy momentum

$$-\overline{(M_c^E)''} \frac{\partial (u^E)''}{\partial p} + \overline{(M_c^C)''} \frac{\partial (u^C)''}{\partial p} \tag{10a}$$

References

- An SI, Wang B (2000) Interdecadal change of the structure of the ENSO mode and its impact on the ENSO frequency. *J Clim* 13:2044–2055
- Bonan GB (1996) A land surface model (LSM version 1.0) for ecological, hydrological, and atmospheric studies: technical description and user's guide. NCAR Technical Note NCAR/TN-417+STR, Natl. Cent. For Atmos. Res., Boulder, 150 pp
- Cane MA, Munnich M, Zebiak SE (1990) A study of self-excited oscillations of the tropical ocean–atmosphere system. Part I: Linear analysis. *J Atmos Sci* 47:1562–1577
- Capotondi A, Wittenberg A, Masina S (2006) Spatial and temporal structure of Tropical Pacific interannual variability in 20th century coupled simulations. *Ocean Model.* doi:[10.1016/j.ocemod.2006.02.004](https://doi.org/10.1016/j.ocemod.2006.02.004)
- Carr MT, Bretherton CS (2001) Convective momentum transport over the tropical Pacific: budget estimates. *J Atmos Sci* 58:1673–1693
- Dima IM, Wallace JM, Kraucunas I (2005) Tropical zonal momentum balance in the NCEP reanalyses. *J Atmos Sci* 62:2499–2513
- Fedorov AV, Philander SG (2001) A stability analysis of tropical ocean–atmosphere interactions: bridging measurements and theory for El Niño. *J Clim* 14:3086–3101
- Gregory D, Kershaw R, Inness PM (1997) Parameterization of momentum transport by convection. 2. Tests in single-column and general circulation models. *Quart J Roy Meteor Soc* 123:1153–1183
- Ham Y-G, Kug J-S, Kang I-S (2007) Role of moist energy advection in formulating anomalous Walker Circulation associated with El-Niño. *J Geophys Res* (in press)
- Helfand HM (1979) Effect of cumulus friction on the simulation of the January Hadley circulation by the Glas model of the general-circulation. *J Atmos Sci* 36:1827–1843
- Holtslag AAM, Boville BA (1993) Local versus nonlocal boundary layer diffusion in a global climate model. *J Clim* 6:1825–1842
- Kalnay E, Kanamitsu M, Kistler R, Collins W, Deaven D, Gandin L, Iredell M, Saha S, White G, Woollen J, Zhu Y, Chelliah M, Ebisuzaki W, Higgins W, Janowiak J, Mo KC, Ropelewski C, Wang J, Leetmaa A, Reynolds R, Jenne R, Joseph D (1996) The NCEP/NCAR 40-year reanalysis project. *Bull Am Meteorol Soc* 77:437–471
- Kang I-S, Kug J-S (2002) El Niño and La Niña sea surface temperature anomalies: asymmetry characteristics associated with their wind stress anomalies. *J Geophys Res* 107(D19):4372
- Kershaw R, Gregory D (1997) Parameterization of momentum transport by convection. 1. Theory and cloud modelling results. *Quart J R Meteorol Soc* 123:1133–1151
- Kidson JW (1975) Tropical eigenvector analysis and the Southern Oscillation. *Mon Wea Rev* 103:187–196
- Kirtman BP (1997) Oceanic Rossby wave dynamics and the ENSO period in a coupled model. *J Clim* 10:1690–1704
- Kug J-S, Kang I-S, An S-I (2003) Symmetric and antisymmetric mass exchanges between the equatorial and off-equatorial Pacific associated with ENSO. *J Geophys Res* 108(C8):3284
- Kug J-S, An S-I, Ham Y-G, Kang I-S (2007a) Changes in ENSO teleconnection due to global warming. *Int J Climatol* (submitted)
- Kug J-S, Kang I-S, Choi D-H (2007b) Seasonal climate predictability with tier-one and tier-two prediction systems. *Clim Dyn.* doi:[10.1007/s00382-007-0264-7](https://doi.org/10.1007/s00382-007-0264-7)
- Latif M et al (2003) ENSIP: the El Niño simulation intercomparison project. *Clim Dyn* 18:255–276
- Le Treut H, Li Z-X (1991) Sensitivity of an atmospheric general circulation model to prescribed SST changes: feedback effects associated with the simulation of cloud optical properties. *Clim Dyn* 5:175–187
- Lee M-I, Kang I-S, Kim J-K, Mapes BE (2001) Influence of cloud-radiation interaction on simulating tropical intraseasonal oscillation with an atmospheric general circulation model. *J Geophys Res* 106:14219–14233
- Lee M-I, Kang I-S, Mapes BE (2003) Impacts of cumulus convection parameterization on aqua-planet AGCM simulations of tropical intraseasonal variability. *J Meteorol Soc Jpn* 81:963–992
- Lin JL, Zhang MH, Mapes B (2005) Zonal momentum budget of the Madden–Julian oscillation: the source and strength of equivalent linear damping. *J Atmos Sci* 62:2172–2188
- Lin JL, Mapes BE, Han W (2007) What are the sources of mechanical damping in Matsuno–Gill type models? *J Clim* (in press)
- Mechoso CR, Robertson AW, Barth N, Davey MK, Delecluse P, Gent PR, Ineson S, Kirtman B, Latif M, Le Treut H, Nagai T, Neelin JD, Philander SGH, Polcher J, Schopf PS, Stockdale T, Suarez MJ, Terray L, Thual O, Tribbia JJ (1995) The seasonal cycle over the Tropical Pacific in general circulation models. *Mon Wea Rev* 123:2825–2838
- Nakajima T, Tsukamoto M, Tsushima Y, Numaguti A (1995) Modelling of the radiative processes in an AGCM. In: Matsuno T (ed) *Climate system dynamics and modelling*, vol I–3. University of Tokyo, Tokyo, pp 104–123
- Neale R (2007) The role of convective moisture sensitivity in improving major systematic biases in the Community Climate System Model (CCSM). *WGNE Workshop on Systematic Errors*, San Francisco, February 2007
- Noh Y, Kim HJ (1999) Simulations of temperature and turbulence structure of the oceanic boundary layer with the improved near-surface process. *J Geophys Res Oceans* 104:15621–15634
- Numaguti A, Takahashi M, Nakajima T, Sumi A (1995) Development of an atmospheric general circulation model. In: Matsuno T (ed) *Climate system dynamics and modelling*, vol I–3. University of Tokyo, Tokyo, pp 1–27
- Ogura Y, Phillips NA (1962) Scale analysis of deep and shallow convection in the atmosphere. *J Atmos Sci* 19:1276–1286
- Rotunno R, Klemp JB (1982) The influence of the shear-induced pressure gradient on thunderstorm motion. *Mon Wea Rev* 110:136–151
- Saravanan R, Chang P (2000) Interactions between tropical Atlantic variability and El Niño-southern Oscillation. *J Clim* 13:2177–2194
- Smith TM, Reynolds RW (2004) Improved extended reconstruction of SST (1854–1997). *J Clim* 17:2466–2477
- Stevens DE (1979) Vorticity, momentum and divergence budgets of synoptic-scale wave disturbances in the Tropical Eastern Atlantic. *Mon Wea Rev* 107:535–550
- Thompson SL, Hartmann DL (1979) Cumulus friction—estimated influence on the Tropical Mean Meridional circulation. *J Atmos Sci* 36:2022–2026
- Tiedtke M (1983) The sensitivity of the time-mean large-scale flow to cumulus convection in the ECMWF model. *Workshop on convection in large-scale numerical models*. ECMWF, 28 Nov–1 Dec 1983, pp 297–316
- Tiedtke M (1989) A comprehensive mass flux scheme for Cumulus parameterization in large-scale models. *Mon Wea Rev* 117:1779–1800
- Tung WW, Yanai M (2002a) Convective momentum transport observed during the TOGA COARE IOP. Part II: Case studies. *J Atmos Sci* 59:2535–2549
- Tung WW, Yanai M (2002b) Convective momentum transport observed during the TOGA COARE IOP. Part I: General features. *J Atmos Sci* 59:1857–1871
- Uppala SM, co-authors (2005) The ERA-40 re-analysis. *Quart J R Meteorol Soc* 131:2961–3012. doi:[10.1256/qj.04.176](https://doi.org/10.1256/qj.04.176)
- Wittenberg AT (2002) ENSO response to altered climates. PhD Thesis, Princeton University, 475 pp

- Wittenberg AT, Rosati T, Held I (2003) ENSO in the GFDL coupled model. Eighth annual CCSM workshop, Breckenridge, 24 June 2003
- Wu XQ, Yanai M (1994) Effects of vertical wind shear on the Cumulus transport of momentum—observations and parameterization. *J Atmos Sci* 51:1640–1660
- Wu XQ, Liang XZ, Zhang GJ (2003) Seasonal migration of ITCZ precipitation across the equator: Why can't GCMs simulate it? *Geophys Res Lett* 30(15):1824, doi:[10.1029/2003GL017198](https://doi.org/10.1029/2003GL017198)
- Wu XQ, Deng L, Song X, Zhang GJ (2007) Coupling of convective momentum transport with convective heating in global climate simulations. *J Atmos Sci* 64:1334–1349
- Xie P, Arkin PA (1997) Global precipitation: a 17-year monthly analysis based on gauge observations, satellite estimates, and numerical model outputs. *Bull Am Meteorol Soc* 78:2539–2558
- Zelle H, van Oldenborgh GJ, Burgers GJ, Dijkstra H (2005) El Niño and greenhouse warming: results from ensemble simulations with the NCAR CCSM. *J Clim* 18:4669–4683
- Zhang GJ, Cho HR (1991) Parameterization of the vertical transport of momentum by Cumulus Clouds. 1. Theory. *J Atmos Sci* 48:1483–1492
- Zhang GJ, Mcfarlane NA (1995) Role of convective scale momentum transport in climate simulation. *J Geophys Res* 100:1417–1426
- Zhang GJ, Wu X (2003) Convective momentum transport and perturbation pressure field from a cloud-resolving model simulation. *J Atmos Sci* 60:1120–1139